Stochastic Sequential Convex Programming for Robust Low-thrust Trajectory Design under Uncertainty

Conference Paper · August 2022

CITATIONS
10

READS
1,091

2 authors, including:

Kenshiro Oguri
Purdue University West Lafayette
80 PUBLICATIONS **486** CITATIONS

SEE PROFILE

AAS 22-708

STOCHASTIC SEQUENTIAL CONVEX PROGRAMMING FOR ROBUST LOW-THRUST TRAJECTORY DESIGN UNDER UNCERTAINTY

Kenshiro Oguri* **and Gregory Lantoine†**

Any space trajectories are subject to state uncertainty due to imperfect state knowledge, random disturbances, and partially known dynamical environments. Ideally, such uncertainty and associated risks must be properly quantified and taken into account in the mission design process to ensure a sufficiently low risk of causing hazardous events. However, designing robust trajectories with such low risk guarantees adds an additional dimension, stochasticity, to space trajectory optimization problems, making it one of the most challenging problems in space mission design. To address the challenge, this study develops a framework that designs robust low-thrust trajectories under uncertainty by combining stochastic optimal control, sequential convex programming, and the augmented Lagrangian method, thereby termed *Stochastic Sequential Convex Programming*. The developed framework incorporates the stochastic effects of orbit determination and control execution errors into the mission design process, enabling mission designers to concurrently design a reference trajectory and flight-path control plan while satisfying mission constraints in the presence of uncertainty.

INTRODUCTION

Designing optimal trajectories has been a central problem of space mission design since 1950s. Over the past several decades, many researchers have devoted their efforts to developing methods that determine optimal low-thrust trajectories. These extensive efforts have led to remarkable advancement in analytical and numerical techniques for low-thrust trajectory optimization, including those based on Lawden's primer vector theory (indirect methods),[1,2] on differential dynamic programming (DDP),[3,4] and on direct transcription via multiple shooting or collocation (direct methods)[5,6] solved by nonlinear programming (NLP).

Meanwhile, any space trajectories are subject to state uncertainty due to various possible causes, such as imperfect state knowledge, random disturbances, and partially known dynamical environments. Guaranteeing performance (e.g., safety and cost) under uncertainty is a major concern in any space mission design. Such performance guarantee is particularly important for missions that need to operate in uncertain environments, that are sensitive to uncertain errors, or that require autonomous operations for an extended duration due to long communication delays. For example, considering an interplanetary orbit transfer, the mission designer must find an optimal transfer trajectory that has a sufficiently low risk of causing hazardous events, such as collision with a planetary body during a close flyby (for the spacecraft safety and planetary protection). Ideally, such risks under uncertainty must be quantitatively evaluated and taken into account in the process of

*Assistant Professor, School of Aeronautics and Astronautics, Purdue University, West Lafayette, Indiana, 47907.
†Mission Design Engineer, Jet Propulsion Laboratory, California Institute of Technology, Pasadena, CA 91109.

mission design. However, the current practice in mission design usually mitigates such risks in a rather heuristic manner, such as by adding extra deterministic margins to the original constraints (e.g., extra propellant mass and planetary flyby impact radius) and by enforcing coasting arcs on sensitive locations on the reference trajectory.[7,8]

The goal of this study is to develop a framework that designs robust low-thrust trajectories under uncertainty. A promising approach to this problem is the application of stochastic optimal control. Along this line, an increasing number of approaches have been proposed, including Refs. 9–14, producing initial yet promising results of the use of stochastic optimal control for trajectory optimization under uncertainty (see Introduction of Ref. 12 for a literature review on this with more details). The authors' previous work in Ref. 13 develops a framework that combines stochastic optimal control and sequential convex programming, termed *Stochastic Sequential Convex Programming*, to design robust solar-sail trajectories under orbit determination (OD) and control errors, which is successfully applied to the interplanetary cruise trajectory design of the NEA Scout mission.

The present study further extends our prior work to develop a solution method for the design of robust optimal low-thrust trajectories under uncertainty. To solve low-thrust problems, unlike solar-sail propulsion, the mass-flow equation must be included in the system dynamics, and the stochastic nature of the mass variable needs to be appropriately taken into account of the framework. Furthermore, the thrust magnitude must be constrained below a maximum thrust level while accommodating flight path control efforts that are necessary to make corrections to the stochastic, erroneous trajectories. Note that, while some existing studies (e.g., Refs. 9, 11, 14) address a similar problem, they do not consider the mass-flow equation and the stochasticity of the mass in their formulation; also, these study only consider a two-dimensional transfer problem with no navigation uncertainty, which makes the applicability of their approach to practical missions unclear.

In addition to these new analytical developments, this study also extends our framework to multi-phase problems. The capability of handling multi-phase problems is a key to designing complex space missions that involve planetary gravity assists, flybys, and gravitational captures/escapes. In particular, this paper presents a formulation to incorporate gravity assists (GAs) into the framework of Stochastic Sequential Convex Programming based on a patched-conic GA model.

The developed Stochastic Sequential Convex Programming framework is applied to two interplanetary transfer scenarios: Earth-Mars transfer and Earth-Mars-Ceres transfer with a gravity assist at Mars. For both scenarios, the framework is shown to successfully design robust optimal reference trajectories and flight path control (FPC) plans (i.e., sequences of feedback control policies). Nonlinear Monte Carlo simulations demonstrate the robustness of the designed trajectories and FPC plans in the original, nonlinear stochastic dynamics.

DYNAMICS

Low-Thrust Engine Model

We assume a constant specific impulse engine as our low-thrust propulsion system, and denote its acceleration term by $\boldsymbol{u} \in \mathbb{R}^3$. The magnitude of the low-thrust acceleration is constrained by the engine's maximum thrust $T_{\max}$ divided by the spacecraft mass m, as in the following equation:

$$\|\boldsymbol{u}\|_2 \leq \frac{T_{\max}}{m}, \tag{1}$$

where $\|\cdot\|_2$ denotes the 2-norm operator. The mass decreases over time at a rate proportional to the thrust magnitude, i.e., $m\|\boldsymbol{u}\|_2$, as:

$$\dot{m} = -\frac{m\|\boldsymbol{u}\|_2}{g_0 I_{\mathrm{sp}}}, \tag{2}$$

where $g_0 (\approx 9.81 \times 10^{-3}\,\mathrm{km/s^2})$ is the standard gravitational acceleration; I_{sp} is the specific impulse of our low-thrust engine.

This study introduces another mass variable,

$$z \triangleq \ln m, \tag{3}$$

to resolve the coupling of the mass and the control in the mass flow equation, which will aid in our convex formulation. This approach is also employed in Ref. 15. With this variable, the mass flow equation is equivalently rewritten as:

$$\dot{z} = -\frac{1}{g_0 I_{sp}}\|\boldsymbol{u}\|_2 . \tag{4}$$

Note that, with this new mass variable, the control magnitude constraint Eq. (1) becomes:

$$\|\boldsymbol{u}\|_2 \leq T_{\max} e^{-z}. \tag{5}$$

Equations of Motion

Let $\boldsymbol{x} \in \mathbb{R}^{n_x}$ be the state of our system, defined as follows:

$$\boldsymbol{x} = \begin{bmatrix} \boldsymbol{x}_{\mathrm{orb}} \\ z \end{bmatrix} \tag{6}$$

where $\boldsymbol{x}_{\mathrm{orb}} \in \mathbb{R}^{n_x-1}$ represents the orbital state. Our equations of motion are expressed in a generic form as follows:

$$\dot{\boldsymbol{x}} = \boldsymbol{f}(\boldsymbol{x}, \boldsymbol{u}, t) = \begin{bmatrix} \boldsymbol{f}_0(\boldsymbol{x}, t) \\ 0 \end{bmatrix} + \begin{bmatrix} F(\boldsymbol{x}_{\mathrm{orb}})\boldsymbol{u} \\ -\frac{1}{g_0 I_{sp}}\|\boldsymbol{u}\|_2 \end{bmatrix} \tag{7}$$

where $\boldsymbol{f}_0(\cdot,\cdot) : \mathbb{R}^{n_x} \times \mathbb{R} \mapsto \mathbb{R}^{n_x-1}$ represents natural orbital dynamics; $F(\cdot) : \mathbb{R}^{n_x-1} \mapsto \mathbb{R}^{(n_x-1)\times 3}$ provides a control influence matrix that maps the acceleration to the rate of the state change. The natural dynamics are expressed as a sum of Keplerian motion and perturbed motion, i.e.,

$$\boldsymbol{f}_0(\boldsymbol{x}, t) = \boldsymbol{f}_{\mathrm{kep}}(\boldsymbol{x}_{\mathrm{orb}}) + F(\boldsymbol{x}_{\mathrm{orb}})\boldsymbol{a}_{\mathrm{pert}}(\boldsymbol{x}, t), \tag{8}$$

where $\boldsymbol{f}_{\mathrm{kep}}(\cdot) : \mathbb{R}^{n_x-1} \mapsto \mathbb{R}^{n_x-1}$ represents the Keplerian dynamics and $\boldsymbol{a}_{\mathrm{pert}}(\cdot,\cdot) : \mathbb{R}^{n_x} \times \mathbb{R} \mapsto \mathbb{R}^3$ the perturbing acceleration. Eq. (7) encompasses equations of motion describing low-thrust orbital dynamics (+ mass flow rate) in various coordinate systems.

Among various possible coordinate systems (e.g., Cartesian, spherical, equinoctial, etc), the Cartesian coordinate system is chosen in this study. Hence, our orbital state and the dynamics functions are given by:

$$\boldsymbol{x}_{\mathrm{orb}} = \begin{bmatrix} \boldsymbol{r} \\ \boldsymbol{v} \end{bmatrix}, \quad \boldsymbol{f}_{\mathrm{kep}}(\boldsymbol{x}_{\mathrm{orb}}) = \begin{bmatrix} \boldsymbol{v} \\ -\frac{\mu}{\|\boldsymbol{r}\|_2^3}\boldsymbol{r} \end{bmatrix}, \quad F = \begin{bmatrix} 0_{3\times 3} \\ I_3 \end{bmatrix} \tag{9}$$

where $\boldsymbol{r} \in \mathbb{R}^3$ and $\boldsymbol{v} \in \mathbb{R}^3$ are the spacecraft position and velocity in Cartesian coordinates, respectively; μ is the gravitational parameter of the central body.

STOCHASTIC OPTIMAL CONTROL FORMULATION

In this section, a stochastic optimal control formulation of our problem is presented in a generic form. Our formulation incorporates the influence of major uncertain errors in space missions (injection error, maneuver execution error, and OD error) as well as the corrective effect of flight-path control efforts (i.e., performing trajectory corrections based on OD results).

Nonlinear Stochastic System

To incorporate uncertain errors and flight-path controls in our mission design process, one of the most straightforward approaches is to express our system via nonlinear stochastic differential equations (SDEs). Based on the equations of motion Eq. (7), our stochastic system can be formally expressed via a set of nonlinear SDEs as:

$$\mathrm{d}\boldsymbol{x} = \boldsymbol{f}(\boldsymbol{x}, \boldsymbol{u}, t)\mathrm{d}t + g_c(\boldsymbol{x}, \boldsymbol{u})\mathrm{d}\boldsymbol{w}(t), \tag{10}$$

where $g_c(\cdot,\cdot) : \mathbb{R}^{n_x} \times \mathbb{R}^3 \mapsto \mathbb{R}^{n_x \times n_w}$ represents the intensity of disturbances, mapping $\mathrm{d}\boldsymbol{w}(t)$ to the random variation of the state; $\mathrm{d}\boldsymbol{w}(t) : \mathbb{R} \mapsto \mathbb{R}^{n_w}$ is a standard Brownian motion vector, i.e., $\mathbb{E}[\mathrm{d}\boldsymbol{w}] = 0$ and $\mathbb{E}\left[\mathrm{d}\boldsymbol{w}(t)\mathrm{d}\boldsymbol{w}^\top(t)\right] = I\mathrm{d}t$. Recall from Eq. (7) that $\boldsymbol{f}(\cdot)$ represents the system dynamics under low-thrust control. The form $g_c(\cdot)\mathrm{d}\boldsymbol{w}$ encompasses various types of disturbances, including unmodeled external perturbations (e.g., solar radiation pressure) and control execution errors such as those characterized by the Gates model.[16]

Nonlinear Stochastic System with Output Feedback

To mathematically model the navigation process and flight-path controls in our formulation, this study considers the output feedback control model, where the deviation of the state from its nominal value is corrected by a feedback controller (i.e., flight-path control) based on imperfect state knowledge (i.e., OD estimate with uncertainty about the true state).

Orbit Determination Model We model our OD process as a sequence of filtering processes with discrete-time observations. Assuming that a set of spacecraft tracking data becomes available at time t_k, our observation process is given by:

$$\boldsymbol{y}_k = \boldsymbol{f}_o(\boldsymbol{x}_k, t_k) + g_o(\boldsymbol{x}_k)\boldsymbol{v}_k, \quad k = 0, 1, ..., N \tag{11}$$

where $\boldsymbol{y}_k \in \mathbb{R}^{n_y}$ is the measurement; $\boldsymbol{f}_o(\cdot,\cdot) : \mathbb{R}^{n_x} \times \mathbb{R} \mapsto \mathbb{R}^{n_y}$ and $g_o(\cdot) : \mathbb{R}^{n_x} \times \mathbb{R} \mapsto \mathbb{R}^{n_y \times n_y}$ model the observation process. $\boldsymbol{v}_k \in \mathbb{R}^{n_y}$ is measurement noise, modeled as a sequence of independent and identically distributed (i.i.d.) standard Gaussian random vectors, i.e., $\mathbb{E}[\boldsymbol{v}_k] = 0$ and $\mathbb{E}\left[\boldsymbol{v}_i \boldsymbol{v}_j^\top\right] = \delta_{i,j} I$, where $\delta_{i,j}$ is the Kronecker delta.

At time t_k, the current state estimate, $\hat{\boldsymbol{x}}_k$, is obtained by a filtering process with the past observations $\boldsymbol{y}_i (i = 0, 1, ..., k)$ as follows:

$$\hat{\boldsymbol{x}}_k = \mathcal{F}_k(\hat{\boldsymbol{x}}_0^-, \boldsymbol{y}_i : i = 0, 1, ..., k), \tag{12}$$

where the "$-$" superscript indicates a quantity right before the measurement update. The initial state distribution, $\boldsymbol{x}_0$, and its estimate, $\hat{\boldsymbol{x}}_0^-$, are assumed to be known (or be estimated conservatively). The estimation error is denoted by $\tilde{\boldsymbol{x}}_k = \boldsymbol{x}_k - \hat{\boldsymbol{x}}_k$.

Flight-path Control Model Flight-path controls are a collection of efforts that drive the orbital state deviation back to the nominal trajectory, planed based on imperfect OD results (the true state is not available in reality). Hence, this study models flight-path controls over the course of a trajectory by a sequence of feedback policies that compute necessary control modifications based on a history of state estimates given by Eq. (12). The feedback policies are thus expressed as:

$$\boldsymbol{u}_k = \pi_k(\boldsymbol{x}_k^*, \boldsymbol{u}_k^*, \Omega_k, \hat{\boldsymbol{x}}_i : i = 0, 1, ..., k-1), \tag{13}$$

where Ω_k denotes a set of parameters used to compute the corrective controls $\boldsymbol{u}_k$ according to the policy π_k. $\boldsymbol{x}^*$ and $\boldsymbol{u}^*$ denote the nominal trajectories of the state and control, respectively.

Original Problem

Cost Function A common cost function in space trajectory optimization is the total control effort. However, we may not employ $J = \sum \|\boldsymbol{u}_k\|_2$ in our stochastic problem because it is not well-defined for numerical optimization due to the randomness of $\boldsymbol{u}_k$ under the feedback policy Eq. (13). Thus, this study considers minimizing the p-quantile of the closed-loop control effort, i.e.,

$$J = \sum_{k=0}^{N} Q_{\|\boldsymbol{u}_k\|_2}(p) \tag{14}$$

where $Q_X(p)$ is the quantile function of a random variable X evaluated at probability p. A formal definition of $Q_X(p)$ is given by

$$Q_X(p) = \min\{x \in \mathbb{R} \mid \mathbb{P}[X \leq x] \geq p\}. \tag{15}$$

Constraints The constraints considered in this study include path constraints and terminal constraints. As our state and control are subject to uncertainty, those constraints are not deterministic anymore and need to be treated stochastically.

In particular, we consider a class of probabilistic constraints called chance constraints to formulate our path constraints, as they naturally represent stochastic analogs of deterministic constraints classically considered in mission design. Intuitively, a chance constraint imposes a bound on the probability that a particular constraint to be satisfied (i.e., no collision with an obstacle with a probability greater than 99.9%); see, for instance, Ref. 12 and references therein, for the use of chance constraints in the context of space trajectory optimization. Mathematically, path chance constraints imposed on discrete-time state and control at time t_k are expressed as:

$$\mathbb{P}[c_j(\boldsymbol{x}_k, \boldsymbol{u}_k, t_k) \leq 0] \geq 1 - \varepsilon_j, \tag{16}$$

where $\mathbb{P}[\cdot]$ denotes the probability operator, $c_j(\cdot) : \mathbb{R}^{n_x} \times \mathbb{R}^3 \times \mathbb{R} \mapsto \mathbb{R}$ represents the j-th nonlinear constraint function, and ε_j is a risk bound associated with the j-th constraint (e.g., $\varepsilon_j = 0.001$ for 99.9% confidence). Since our low-thrust trajectory optimization problem must ensure the satisfaction of the control magnitude constraint (with the mass variable z, Eq. (5)), its counterpart in the stochastic formulation is given by:

$$\mathbb{P}\left[\|\boldsymbol{u}_k\|_2 \leq T_{\max} e^{-z_k}\right] \geq 1 - \varepsilon_u, \ \forall k. \tag{17}$$

In a similar manner, we model our terminal constraints as distributional constraints that ensure that our final state is within a prescribed region. Specifically, our terminal constraint is formulated

to make sure that the designed trajectory nominally achieves the target $\boldsymbol{x}_f$ with prescribed accuracy represented by the final covariance P_f:

$$\boldsymbol{x}_N^* - \boldsymbol{x}_f = 0, \quad P_N \preceq P_f \tag{18}$$

where P_N denotes the covariance of the final state under the action of corrective controls Eq. (13).

Thus, our original problem can be expressed as in Problem 1.

Problem 1 (Original problem)**.** *Find* $\boldsymbol{x}^*(t), \boldsymbol{u}_k^*, \pi_k$*, and* Ω_k*,* $\forall k$ *that minimize the cost Eq.* (14) *subject to the dynamical constraint Eq.* (10)*, path chance constraints Eq.* (17)*, and terminal constraint Eq.* (18) *under a sequence of flight-path controls determined by Eq.* (13) *with the state estimates Eq.* (12) *based on observations Eq.* (11)*.*

STOCHASTIC SEQUENTIAL CONVEX PROGRAMMING

In general, Problem 1 is expensive, if possible at all, to solve. A major bottleneck of this lies in the process of nonlinear *uncertainty quantification* (UQ) to evaluate the statistics of the state, cost, and constraints under uncertainty. Nonlinear UQ is normally very expensive except for some special cases. In trajectory optimization problems for which no closed-form solution is available, we must iteratively perform such expensive nonlinear UQ processes to evaluate the functions and their gradients about a reference solution. This requires an efficient and reliable solution method.

Among multiple possible approaches, we develop a solution method based on sequential convex programming to solve our problem. The solution method combines linear covariance steering with output feedback[17] and successive convexification for nonlinear trajectory optimization.[18,19]

The proposed approach approximately formulates the originally expensive problem in a convex form at each successive iteration. At each iteration, the original problem is approximated as a convex subproblem, which is solved with guaranteed convergence to the global optimum of the approximated problem due to the convex property. Once the convergence of a convex subproblem is achieved, then the subproblem solution is used as a new reference trajectory for the next iteration. Leveraging the reliability and efficiency of convex programming, this solution method provides us with a vehicle for overcoming the major bottleneck of numerical solutions to nonlinear stochastic optimal control problems, in exchange for approximate dynamical evolution of the stochastic state deviations from the reference trajectory. Note that the dynamical feasibility of the reference trajectory is not compromised in our solution method (i.e., the designed reference trajectory satisfies the nonlinear dynamics up to the user-specified tolerance).

The convex subproblem that approximates Problem 1 is formulated in the following subsections.

Linear State Statistics Dynamics

Linear, Discrete-time System We define s as $s \triangleq \frac{\mathrm{d}t}{\mathrm{d}\tau}$ and normalize the time by s with $\tau \in [0, 1]$:

$$\mathrm{d}\boldsymbol{x} = s\boldsymbol{f}(\boldsymbol{x}, \boldsymbol{u}, \tau)\mathrm{d}\tau + \sqrt{s} g_c(\boldsymbol{x}, \boldsymbol{u}, t)\mathrm{d}\boldsymbol{w}(\tau). \tag{19}$$

The initial state and initial state estimate are assumed to be Gaussian-distributed about the reference, i.e., $\boldsymbol{x}_0 \sim \mathcal{N}(\boldsymbol{x}_0^*, P_0)$ and $\hat{\boldsymbol{x}}_0 \sim \mathcal{N}(\boldsymbol{x}_0^*, \hat{P}_0^-)$. Following the same procedure as presented in Ref. 13, Eq. (19) can be linearized and discretized (see Ref. 13 for the definition of $A_k, B_k, \boldsymbol{h}_k, G_k$, and $\boldsymbol{w}_k$):

$$\boldsymbol{x}_{k+1} = A_k \boldsymbol{x}_k + B_k \boldsymbol{u}_k + \boldsymbol{h}_k + G_k \boldsymbol{w}_k, \tag{20}$$

Linear Flight-path Control Model For convex formulation, the flight-path control policies, presented in Eq. (13), are simplified to be a sequence of affine filtered state feedback controllers. That is, $\boldsymbol{u}_k$ is calculated as a linear feedback control of the current state estimate $\hat{\boldsymbol{x}}_k$:

$$\boldsymbol{u}_k = \boldsymbol{u}_k^* + K_k(\hat{\boldsymbol{x}}_k - \boldsymbol{x}_k^*), \tag{21}$$

where K_k are feedback gain matrices to be determined by numerical optimization.

Filtered State Dynamics Since the state is initially Gaussian-distributed and obeys the linear dynamics in a convex subproblem, the optimal, unbiased state estimate can be obtained by the Kalman filter. Thus, the filtration process Eq. (12) in a subproblem is given as:

$$\begin{cases} \hat{\boldsymbol{x}}_k^- = A_{k-1}\hat{\boldsymbol{x}}_{k-1} + B_{k-1}\boldsymbol{u}_{k-1} + \boldsymbol{h}_{k-1} \\ \tilde{P}_k^- = A_{k-1}\tilde{P}_{k-1}A_{k-1}^\top + G_{k-1}G_{k-1}^\top, \end{cases} \quad \text{(time update)}$$
$$\begin{cases} \hat{\boldsymbol{x}}_k = \hat{\boldsymbol{x}}_k^- + L_k(\boldsymbol{y}_k - C_k\hat{\boldsymbol{x}}_k^-) \\ \tilde{P}_k = (I - L_kC_k)\tilde{P}_k^-(I - L_kC_k)^\top + L_kD_kD_k^\top L_k^\top, \end{cases} \quad \text{(measurement update)} \tag{22}$$

where $\tilde{P}_k$ denotes the estimate error covariance; L_k is the Kalman gain; C_k and D_k are the linearized measurement equation about the reference, given by

$$\tilde{P}_k \triangleq \mathrm{Cov}\left[\tilde{\boldsymbol{x}}_k\right], \quad L_k \triangleq \tilde{P}_k^- C_k^\top (C_k\tilde{P}_k^- C_k^\top + D_kD_k^\top)^{-1}, \quad C_k \triangleq \frac{\partial \boldsymbol{f}_o^*}{\partial \boldsymbol{x}}, \quad D_k \triangleq \frac{\partial \boldsymbol{g}_o^*}{\partial \boldsymbol{x}}. \tag{23}$$

As classically known in estimation theory, $\tilde{P}_k$ and L_k can be computed *a priori* for linear systems.

Combining the two equations in Eq. (22), the filtered state process under stochastic error and measurement noise is written as:

$$\hat{\boldsymbol{x}}_{k+1} = A_k\hat{\boldsymbol{x}}_k + B_k\boldsymbol{u}_k + \boldsymbol{h}_k + L_{k+1}\tilde{\boldsymbol{y}}_{k+1}^-, \tag{24}$$

where $\tilde{\boldsymbol{y}}_k^-$ (often called *innovation process*) is defined as in Eq. (25). Eq. (25) also includes the expression for its covariance, denoted by $P_{\tilde{y}_k^-}$, which is derived by noting the independency between $\tilde{\boldsymbol{x}}_k, \boldsymbol{w}_i, \boldsymbol{v}_i, \forall i = 1, 2, ..., k-1$.

$$\tilde{\boldsymbol{y}}_k^- = \boldsymbol{y}_k - C_k\hat{\boldsymbol{x}}_k^- (= C_k\tilde{\boldsymbol{x}}_k + D_k\boldsymbol{v}_k), \quad P_{\tilde{y}_k^-} \triangleq \mathrm{Cov}\left[\tilde{\boldsymbol{y}}_k^-\right] = C_k\tilde{P}_k^- C_k^\top + D_kD_k^\top. \tag{25}$$

State and Control Statistics Now, we are ready to analytically express the dynamics of the state statistics—mean and covariance—under control. Relevant existing studies propose different approaches to express the dynamics in a convex form, including those based on block-matrix formulation[11,13] and on a relaxation that employs Schur complement lemma.[14] A previous study of the present authors takes the block-matrix approach.[13]

However, in this paper we propose a different formulation based on the square-root covariance expression, which has the following two advantages over the existing approaches: 1) better numerical conditions—as discussed in Ref. 20, using the full covariance matrix (rather than its square-root form) is prone to numerically ill-conditioned problems; 2) greater flexibility in the implementation—the block-matrix formulation can be highly restrictive (or non-intuitive) in expressing the covariance dynamics of complex optimization problems (e.g., multi-phase problems). The analytical expression derived in this study is summarized in Lemma 1.

Lemma 1. *Let X_k and S_k be defined as $X_k X_k^\top = \hat{P}_k$ and $S_k S_k^\top = P_{u_k}$, then the time evolution of the filtered state statistics under Eqs.* (21) *and* (24) *is given by:*

$$\begin{aligned} \bar{\boldsymbol{x}}_{k+1} &= A_k \bar{\boldsymbol{x}}_k + B_k \bar{\boldsymbol{u}}_k + \boldsymbol{h}_k, && \text{(mean)} \\ X_{k+1} &= [A_k X_k + B_k S_k,\ L_{k+1}(P_{\tilde{y}_k^-})^{1/2}], && \text{(covariance)}, \end{aligned} \tag{26}$$

where $(P_{\tilde{y}_k^-})^{1/2}$ satisfies $(P_{\tilde{y}_k^-})^{1/2}(P_{\tilde{y}_k^-})^{1/2^\top} = P_{\tilde{y}_k^-}$.

Proof. See Appendix. □

Once X_k and S_k are obtained, the feedback gain matrices K_k are recovered analytically by inverting $S_k = K_k X_k$. Note that this process is inexact because it only allows a least-square solution $K_k = S_k(X_k^\top X_k)^{-1} X_k^\top$ due to the rectangular shape of X_k. However, the nonlinear Monte Carlo simulations in the numerical examples of this paper show that the resulting gain matrices K_k successfully control the stochastic states while satisfying the constraints. Finding an exact gain matrix retrieval formulation is an important aspect of the continued study.

Remark 1. *With Eq.* (26)*, $\bar{\boldsymbol{x}}_k$ and X_k for every k are affine in $\bar{\boldsymbol{x}}_i$, $\bar{\boldsymbol{u}}_i$, X_i, and S_i, $i = 0, 1, ..., k-1$.*

Remark 2. *The size of X_k is not constant, and its number of columns increases every time step by n_x, i.e., $X_k \in \mathbb{R}^{n_x \times k n_x}$. Thus, the computational complexity of the subproblem increases quadratically in N. This computational complexity is in the same order as those developed in Ref. 11, 13.*

Constraint Function

Let us first formulate our probabilistic constraint functions Eqs. (17) and (18) in deterministic, convex forms, followed by the convex formulation of the cost function Eq. (14).

A convex formulation of terminal constraint Eq. (18) is readily available by slightly modifying the results of existing studies (e.g., Refs. 13, 17), yielding:

$$\bar{\boldsymbol{x}}_N - \boldsymbol{x}_f = 0, \quad \left\| (P_f - \tilde{P}_N)^{-1/2} X_N \right\| - 1 \leq 0. \tag{27}$$

The convex formulation of the control magnitude constraints Eq. (17) requires more analytical efforts. Note that the convex formulation proposed in Ref. 11, which assumes constant spacecraft mass over transfers, is not applicable here because of the inclusion of the spacecraft mass as a state variable. In particular, the main issue that needs to be addressed is the stochasticity of the mass variable z in our formulation. Due to the stochasticity of the mass variable, it is not easy to convert our norm chance constraints Eq. (17) into a deterministic form because these chance constraints involve two different (but not independent) random variables $\boldsymbol{u}_k$ and z_k.

We address this by introducing an additional deterministic control variable, denoted by Γ_k. With this new variable, Eq. (17) is equivalently expressed as:

$$\mathbb{P}\left[\|\boldsymbol{u}_k\|_2 \leq \Gamma_k \ \wedge \ \Gamma_k \leq T_{\max} \exp\left(-z_k\right) \right] \geq 1 - \varepsilon_u, \ \forall k. \tag{28}$$

It is clear by applying the Boole's inequality[21] that Eq. (28) is satisfied if the following two chance constraints are satisfied:

$$\mathbb{P}\left[\|\boldsymbol{u}_k\|_2 \leq \Gamma_k \right] \geq 1 - \frac{\varepsilon_u}{2}, \ \forall k, \tag{29}$$

$$\mathbb{P}\left[\Gamma_k \leq T_{\max} \exp\left(-z_k\right) \right] \geq 1 - \frac{\varepsilon_u}{2}, \ \forall k. \tag{30}$$

Table 1. Magnitude constraint tightness comparison

Approach	$\{\varepsilon, n_u\} =$	$\{1.0\text{E}{-2}, 3\}$	$\{1.0\text{E}{-3}, 3\}$	$\{1.0\text{E}{-2}, 4\}$	$\{1.0\text{E}{-3}, 4\}$
This study [Eq. (32)]	$n_\sigma =$	3.3682	4.0331	3.6437	4.2973
Ridderhof et.al.[11] [Eq. (34)]	$n'_\sigma =$	4.7669	5.4490	5.0349	5.7169

Among Eqs. (29) and (30), we first present a deterministic, convex formulation of Eq. (29) in the following. The derivation relies on Lemma 2. Using the result stated in Lemma 2, it is straightforward to verify that Eq. (29) holds if $\|\bar{\boldsymbol{u}}_k\|_2 + n_\sigma\left(\frac{\varepsilon_u}{2}, n_u\right)\sqrt{\lambda_{\max}(P_{u_k})} \leq \Gamma_k$ is true. Thus, recalling $S_k S_k^\top = P_{u_k}$, this can be equivalently rewritten in a convex form as:

$$\|\bar{\boldsymbol{u}}_k\|_2 + n_\sigma\left(\frac{\varepsilon_u}{2}, n_u\right)\|S_k\|_2 \leq \Gamma_k. \tag{31}$$

Qualitatively, n_σ represents *how many sigmas are necessary to achieve the magnitude constraint with* $(1-\varepsilon)$ *confidence*. n_σ is computed as in Eq. (32), where the numerical computation of $Q_{X\sim\chi^2(n_u)}(1-\varepsilon)$ is straightforward in modern computer languages, such as `chi2inv`$(1-\varepsilon, n_u)$ in Matlab and `chi2.cdf`$(1-\varepsilon, n_u)$ in Python's `scipy` package.

Lemma 2. *Let* $\boldsymbol{u} \sim \mathcal{N}(\bar{\boldsymbol{u}}, P_u)$ *be an* n_u*-dimensional normal random vector,* $\varepsilon \in (0,1)$*,* $\Gamma > 0$*, and*

$$n_\sigma(\varepsilon, n_u) = \sqrt{Q_{X\sim\chi^2(n_u)}(1-\varepsilon)}, \tag{32}$$

where $Q_{X\sim\chi^2(n_u)}(1-\varepsilon)$ *is the quantile function of the chi-squared distribution with* n_u *degrees of freedom, evaluated at probability* $(1-\varepsilon)$*. Then*

$$\|\bar{\boldsymbol{u}}\|_2 + n_\sigma(\varepsilon, n_u)\sqrt{\lambda_{\max}(P_u)} \leq \Gamma \quad \Rightarrow \quad \mathbb{P}\left[\|\boldsymbol{u}\|_2 \leq \Gamma\right] \geq 1-\varepsilon \tag{33}$$

where $\lambda_{\max}(\cdot)$ *is the largest eigenvalue of a matrix.*

Proof. See Appendix. □

Remark 3. n_σ *given by Eq.* (32) *provides a tighter approximation than the one proposed in Ridderhof et.al.[11] The equivalent of* n_σ *in Ref. 11, denoted by* n'_σ*, is given by:*

$$n'_\sigma = \sqrt{2\ln\frac{1}{\varepsilon}} + \sqrt{n_u} \quad (n_u > 2), \quad n'_\sigma = \sqrt{2\ln\frac{1}{\varepsilon}} \quad (n_u = 1, 2) \tag{34}$$

The values of n_σ *given by Eq.* (32) *(this study) and by Eq.* (34) *(Ridderhof et.al.[11]) coincide when* $n_u = 2$*, whereas Eq.* (32) *yields smaller* n_σ*, and hence tighter constraints, for* $n_u > 2$*. Table 1 compares* n_σ *computed by the two approaches, confirming the tightness of our approximation.*

Next, we discuss formulating Eq. (30) in a deterministic form. Eq. (30) is equivalent to:

$$\mathbb{P}\left[z_k + \ln\left(\frac{\Gamma_k}{T_{\max}}\right) \leq 0\right] \geq 1 - \frac{\varepsilon_u}{2}, \ \forall k, \tag{35}$$

where only z_k is stochastic. This inequality can be expressed by using a quantile function as:

$$Q_{z_k}\left(1-\frac{\varepsilon_u}{2}\right) + \ln\left(\frac{\Gamma_k}{T_{\max}}\right) \leq 0. \tag{36}$$

Let us then evaluate the quantile function of the distribution of z_k. Since our formulation uses the ZoH control discretization, z_k is given by (recall the differential equation for z in Eq. (4)):

$$z_{k+1} = z_0 + \sum_{i=0}^{k}(z_{i+1} - z_i), \quad z_{k+1} - z_k = -b_k \left\|\boldsymbol{u}_k\right\|_2, \quad b_k = \frac{t_{k+1} - t_k}{g_0 I_{\mathrm{sp}}} \ (>0), \tag{37}$$

where $\boldsymbol{u}_k \sim \mathcal{N}(\bar{\boldsymbol{u}}_k, P_{u_k})$, implying that the distribution of $(z_{k+1} - z_k)^2$ may be modeled as a generalized chi-squared distribution. Thus, $Q_{z_k}(\cdot)$ can be evaluated from above as stated in Lemma 3, and therefore Eq. (36) (and hence Eq. (35) also) holds if the following equation is satisfied:

$$z_0 - \sum_{i=0}^{k-1} b_i \max\left[0, \left\|\bar{\boldsymbol{u}}_i\right\|_2 - n_\sigma\left(\frac{\varepsilon_u}{2k}, n_u\right)\sqrt{\lambda_{\max}(P_{u_i})}\right] + \ln\left(\frac{\Gamma_k}{T_{\max}}\right) \leq 0. \tag{38}$$

Lemma 3. *Let z_k obeys the stochastic difference equation Eq.* (37)*, $\boldsymbol{u}_k \sim \mathcal{N}(\bar{\boldsymbol{u}}_k, P_{u_k})$, and $Q_{z_k}(p)$ be the quantile function of z_k evaluated at probability p. Then, $Q_{z_k}(1 - \varepsilon_u/2)$ is evaluated from above as:*

$$Q_{z_k}\left(1 - \frac{\varepsilon_u}{2}\right) \leq z_0 - \sum_{i=0}^{k-1} b_i \max\left[0, \left\|\bar{\boldsymbol{u}}_i\right\|_2 - n_\sigma\left(\frac{\varepsilon_u}{2k}, n_u\right)\sqrt{\lambda_{\max}(P_{u_i})}\right] \tag{39}$$

Proof. See Appendix. □

Although a deterministic expression of the mass variable chance constraints is obtained as in Eq. (38), it is clearly non-convex. On the other hand, the mass variable z_k only appears in Eq. (38) and only affects the value of Γ_k, i.e., the upper bound of the control magnitude. This observation leads us to take an approximation approach where Γ_k are given as constants estimated from previous iteration, in such a manner that Γ_k satisfy Eq. (38) with equalities based on $\bar{\boldsymbol{u}}_k$ and P_{u_k} obtained in the previous iteration. That is, Γ_k are computed before each iteration as:

$$\Gamma_k^{(j+1)} = T_{\max} \exp\left\{-z_0 + \sum_{i=0}^{k-1} b_i \max\left[0, \left\|\bar{\boldsymbol{u}}_i^{(j)}\right\|_2 - n_\sigma\left(\frac{\varepsilon_u}{2k}, n_u\right)\sqrt{\lambda_{\max}(P_{u_i}^{(j)})}\right]\right\}, \tag{40}$$

where the superscript (j) indicates the solution obtained by the j-th iteration.

Cost Function

By extending Lemma 2, Eq. (14) can be readily expressed in a deterministic, convex form as:

$$J_{\mathrm{cvx}} = \sum_{k=0}^{N} \left\|\bar{\boldsymbol{u}}_k\right\|_2 + n_\sigma\left(1 - p, n_u\right)\left\|S_k\right\|_2. \tag{41}$$

Convex Subproblem

Our convex subproblem is thus formulated as in Problem 2.

Problem 2 (Convex subproblem)**.** *Find $\bar{\boldsymbol{x}}_k$, $\bar{\boldsymbol{u}}_k$, X_k, and S_k, $\forall k$ that minimize the cost Eq.* (41) *subject to the mean and covariance dynamics Eq.* (26)*, terminal constraint Eq.* (27)*, and path chance constraints Eq.* (31)*, where Γ_k are given by Eq.* (40) *using the previous iteration result.*

Sequential Convex Programming with Augmented Lagrangian Method

Our solution method alternately constructs and solves the convex subproblem Problem 2 while updating the reference trajectory based on the subproblem result, marching toward the overall convergence. While each subproblem is guaranteed to converge due to the convexity, the reference updating process needs to have a mechanism to check the solution validity in the original nonlinear system, as each iteration relies on a linearized system. To address this, this study adopts an approach proposed in Ref. 18, which proves the convergence of their approach to a local optimum of the original problem and its convergence rate.

An important aspect of the approach is to avoid unfavorable situations that are known to occur in general successive convexification frameworks, if naïvely formulated. As detailed in Ref. 18, a naïve formulation may lead to *artificial unboundedness* and *artificial infeasibility*. This study bases our solution method on their approach with some modifications. Specifically, to mitigate artificial unboundedness, the trust region method is employed to bound the feasible regions of $\bar{\boldsymbol{x}}_k$ at each iteration within the trust region Δ_x:

$$\|\bar{\boldsymbol{x}}_k - \boldsymbol{x}_k^*\|_\infty \leq \Delta_x, \ \forall k \tag{42}$$

To avoid artificial infeasibility, the augmented Lagrangian method[22] is utilized to temporarily allow constraint violations and penalize the violations by augmenting the cost function in each subproblem. Note that it is not necessary (nor effective) to relax and penalize all the constraints; we should do so for only critical constraints that may render the subproblem infeasible otherwise. Expressing a collection of functions for relaxed constraints by g_i^{eq} $(i = 1, 2, ..., N_{\mathrm{eq}})$ and g_i^{ineq} $(i = 1, 2, ..., N_{\mathrm{ineq}})$ (equality and inequality, respectively), the relaxed constraints are given by

$$g_i^{\mathrm{eq}} = \xi_i, \quad g_i^{\mathrm{ineq}} \leq \zeta_i, \tag{43}$$

where $\xi_i, \zeta_i \in \mathbb{R}$ are slack variables that measure the constraint violation. These slack variables are then used in the augmented cost function to penalize the constraint violation as:

$$J_{\mathrm{cvx,aug}} = J_{\mathrm{cvx}} + \sum_{i=1}^{N_{\mathrm{eq}}} \left(\lambda_i \xi_i + \frac{1}{2} c \xi_i^2 \right) + \sum_{i=1}^{N_{\mathrm{ineq}}} \left[\mu_i \max\{0, \zeta_i\} + \frac{1}{2} c (\max\{0, \zeta_i\})^2 \right], \tag{44}$$

where $c \in \mathbb{R}$ is a penalty weight, $\lambda_i, \mu_i \in \mathbb{R}$ are Lagrange multiplier.

Problem 3 summarizes our modified convex subproblem that incorporates these two aspects.

Problem 3 (Convex subproblem with trust regions and augmented Lagrangian penalty)**.** *Find* $\bar{\boldsymbol{x}}_k$*,* $\bar{\boldsymbol{u}}_k$*,* X_k*, and* S_k $\forall k$*,* ξ_i $(i = 1, 2, ..., N_{\mathrm{eq}})$*, and* ζ_i $(i = 1, 2, ..., N_{\mathrm{ineq}})$ *that minimize the penalized cost Eq.* (44) *subject to the trust region constraint Eq.* (42) *and the non-relaxed constraints among Eqs.* (26)*,* (27) *and* (31)*, where* Γ_k *are given by Eq.* (40) *using the previous iteration result.*

At each iteration after a subproblem is solved, the parameters c, ξ, ζ are updated if the associated constraints are violated, according to the following formula[22]

$$c_i^{(j+1)} = \gamma_c c_i^{(j)} \quad \lambda_i^{(j+1)} = \lambda_i^{(j)} + c^{(j)} \xi_i^{(j)}, \quad \mu_i^{(j+1)} = \max\{0, \mu_i^{(j)} + c^{(j)} \xi_i^{(j)}\} \tag{45}$$

where the superscript (j) indicates the solution of the j-th iteration; $\gamma_c (> 1) \in \mathbb{R}$ is a constant. Then, the reference is updated depending on the value of a quantity $\rho^{(j)}$, which represents the ratio

of the actual cost change to the predicted change. If $\rho^{(j)}$ is greater than a prescribed value, the reference $\{\boldsymbol{x}_k^*, \boldsymbol{u}_k^*\}$ is replaced by $\{\bar{\boldsymbol{x}}_k^{(j)}, \bar{\boldsymbol{u}}_k^{(j)}\}$; otherwise, the reference is not changed, and the same convex subproblem is solved with a smaller trust region. See Ref. 18 for more detail on this procedure and its theoretical justification. A key difference in our formulation is the evaluation of the nonlinear cost; our formulation does not take into account the nonlinear cost and penalties that are dependent on stochastic terms, as evaluating these quantities without approximation (i.e., performing exact nonlinear UQ) can be too expensive. Accordingly, only the deterministic components are incorporated in the computation of $\rho^{(j)}$.

EXTENSION TO MULTI-PHASE PROBLEMS

Extension of the developed mission design framework to multi-phase problems is straightforward. We can simply connect each phase via an "event," which may represent a planetary gravity assist, flyby, and rendezvous. The type of the event dictates how the state statistics (mean and covariance) before and after an event are constrained. All the phases, connected via event constraints, are convexified and optimized simultaneously at each iteration of sequential convex programming. As one of the numerical examples of this paper considers a Earth-Mars-Ceres transfer that involves a Mars gravity assist (GA), the GA formulation used in our framework is presented below.

Gravity Assist

A patched-conic GA model[23] is used to model the GA effect as a set of event constraints. In this model, a GA event rotates the spacecraft velocity relative to the planet (i.e., $\boldsymbol{v}_\infty$) while a constraint on the periapsis radius about the planet is imposed. These GA conditions are summarized as:

$$\left\|\boldsymbol{v}_\infty^+\right\|_2 = \left\|\boldsymbol{v}_\infty^-\right\|_2, \quad \boldsymbol{v}_\infty^+ \cdot \boldsymbol{v}_\infty^- = \left\|\boldsymbol{v}_\infty^-\right\|_2^2 \cos\theta, \quad \left\|\boldsymbol{v}_\infty^-\right\|_2 - \sqrt{\frac{\mu_p}{r_{p\,\min}}\left(\frac{1}{\sin\frac{\theta}{2}} - 1\right)} \leq 0 \tag{46}$$

where $\boldsymbol{v}_\infty^\pm$ denotes $\boldsymbol{v}_\infty$ vector before $(-)$ or after $(+)$ the GA, calculated as $\boldsymbol{v}_\infty^\pm = \boldsymbol{v}^\pm - \boldsymbol{v}_p$. The subscript p indicates quantities associated with the planet, i.e., $\boldsymbol{v}_p$: planet velocity, μ_p: planet's gravity constant, and $r_{p\,\min}$: minimum allowable periapsis radius. θ is the turn angle of $\boldsymbol{v}_\infty$ vector due to a GA. The last inequality in Eq. (46) is derived from the classical minimum periapsis constraint.

While Eq. (46) is simple to apply for deterministic problems, it is not suited for stochastic problems because it does not clarify how the state covariance should be mapped across a GA event. Thus, this study derives another form of Eq. (46) that furnishes an explicit formula that maps P_k^- to P_k^+ across a GA event. To this end, we express the rotation of $\boldsymbol{v}_\infty$ via an orthogonal matrix $R \in \mathbb{R}^{3\times3}$ as: $\boldsymbol{v}_\infty^+ = R\boldsymbol{v}_\infty^-$. This way, we can explicitly write the covariance mapping of $\boldsymbol{v}_\infty$ as: $P_{v_\infty^+} = RP_{v_\infty^-}R^\top$, where R is an additional optimization variable.

However, using R as an optimization variable introduces another issue; that is, imposing the orthogonality condition on a matrix variable is non-convex. To address this issue, this study proposes to utilize *Cayley transform*[*] to express the orthogonal matrix R in terms of a skew-symmetric matrix $V \in \mathbb{R}^{3\times3}$ as $R = (I_3 + V)^{-1}(I_3 - V)$, yielding

$$\boldsymbol{v}_\infty^+ = (I_3 + V)^{-1}(I_3 - V)\boldsymbol{v}_\infty^-, \tag{47}$$

[*]For any skew-symmetric matrix A, a matrix Q that satisfies $Q = (I + A)^{-1}(I - A)$ is an orthogonal matrix with its determinant $+1$, i.e., $QQ^\top = I$ and $|Q| = 1$.

where $I_n \in \mathbb{R}^{n\times n}$ is an identity matrix and $V^\top = -V$. It is clear that Eq. (47) automatically satisfies the first constraint of Eq. (46). Assuming the deterministic GA epoch (i.e., no uncertainty in the planet state) and deterministic $\boldsymbol{v}_\infty$ rotation, event constraints at a GA are given by

$$\bar{\boldsymbol{r}}_k^- = \bar{\boldsymbol{r}}_k^+ = \boldsymbol{r}_p, \quad (I_3 + V)(\bar{\boldsymbol{v}}_k^+ - \boldsymbol{v}_p) = (I_3 - V)(\bar{\boldsymbol{v}}_k^- - \boldsymbol{v}_p) \qquad \text{(mean)}, \tag{48a}$$

$$X_k^+ = \begin{bmatrix} I_3 & 0_{3\times3} \\ 0_{3\times3} & (I_3 + V^*)^{-1}(I_3 - V^*) \end{bmatrix} X_k^- \qquad \text{(covariance)} \tag{48b}$$

$$(\bar{\boldsymbol{v}}_k^+ - \boldsymbol{v}_p) \cdot (\bar{\boldsymbol{v}}_k^- - \boldsymbol{v}_p) = \left\|\bar{\boldsymbol{v}}_k^- - \boldsymbol{v}_p\right\|_2^2 \cos\theta \qquad \text{(turn angle)}, \tag{48c}$$

$$\mathbb{P}\left[\left\|\boldsymbol{v}_k^- - \boldsymbol{v}_p\right\|_2 - \sqrt{\frac{\mu_p}{r_{p\,\min}}\left(\frac{1}{\sin\frac{\theta}{2}} - 1\right)} \le 0\right] \ge 1 - \varepsilon_g \qquad \text{(periapsis radius)}, \tag{48d}$$

where V^* is V of the reference trajectory. A chance constraint is imposed on the minimum periapsis to ensure no collision with the planet under uncertain incoming $\boldsymbol{v}_\infty$, where ε_g is the risk bound. As Eqs. (48a) and (48c) are non-convex, these equality constraints are linearized at each iteration for convex subproblem. Eq. (48d) can be rewritten in a deterministic form by using Lemma 2 as:

$$\left\|\bar{\boldsymbol{v}}_k^- - \boldsymbol{v}_p\right\|_2 + n_\sigma\left(\varepsilon_g, 3\right)\left\|[0_{3\times3}\ \ I_3]\, X_k^-\right\|_2 - \sqrt{\frac{\mu_p}{r_{p\,\min}}\left(\frac{1}{\sin\frac{\theta}{2}} - 1\right)} \le 0 \tag{49}$$

A higher-fidelity GA modeling is also possible to incorporate in our framework. For this, extending the formulation proposed in Ref. 24 to stochastic setting would be a straightforward approach, where a GA would be treated as a phase rather than an instantaneous event.

NUMERICAL RESULTS

The developed solution method is applied to two trajectory optimization problems: an Earth-Mars transfer and an Earth-Mars-Ceres transfer with a gravity assist at Mars (both three-dimensional). The objective is to minimize the 99% quantile of the fuel consumption. The position and velocity of the celestial bodies are defined based on the DE430 planetary ephemeris model provided by JPL.

Earth-Mars Transfer

Transfer scenario The Earth-Mars transfer scenario is assumed to depart Earth at 2024 Aug 11 and arrive at Mars with a fixed 500-day time of flight. The spacecraft specifications are assumed to be $I_{\rm sp} = 4000$ [sec], $T_{\max} = 0.5$ [N], and $m(t=0) = 2000$ [kg]. The trajectory is discretized into 31 nodes. Fig. 1 summarizes the deterministic optimal solution with no uncertainty consideration, which is used as the initial guess for solving our stochastic problem. Fig. 1(a) shows the transfer trajectory projected onto the position x-y plane, where the origin is the Sun; Fig. 1(b) shows the control profile for the deterministic optimal trajectory, where α, β are the inertial longitude and latitude of the thrust direction, calculated as: $\alpha = \arctan 2(u_2/u_1)$ and $\beta = \arcsin(u_3)$; $\arctan 2(\cdot)$ is the four-quadrant inverse tangent function.

Major uncertain errors relevant to this scenario include the initial state dispersion, control execution errors, and orbit determination (OD) errors, all of which can be handled within the framework developed in this study. The initial state dispersion is modeled as a Gaussian distribution of covariance $P_0 = \mathrm{blkdiag}(\sigma_{r0}^2 I_3, \sigma_{v0}^2 I_3)$, where $\{\sigma_{r0}, \sigma_{v0}\}$ denote the standard deviations of the

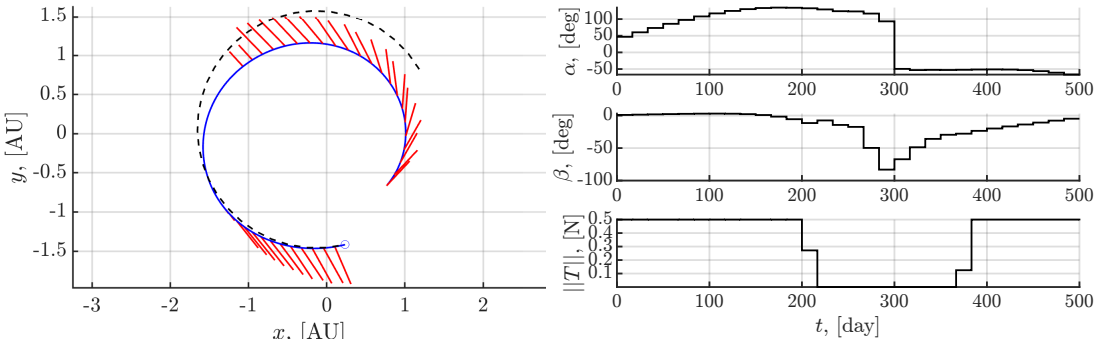

(a) Deterministic optimal trajectory (b) Time history of deterministic optimal control

Figure 1. Deterministic optimal Earth-Mars low-thrust transfer

position and velocity dispersion at the epoch of Earth departure. Their values are assumed to be $\{\sigma_{r0}, \sigma_{v0}\} = \{30,000 \text{ km},\ 30.0 \text{ m/s}\}$.

The execution error is modeled by the Gates model[16] to take into account the pointing and magnitude errors, where the standard deviations of these uncertain errors are assumed to be $\{\sigma^{\text{u}}_{\text{dire}}, \sigma^{\text{u}}_{\text{prop}}\} = \{1 \text{ deg},\ 1\ \%\}$. See Ref. 13 for the detail on formulating the Gates model in the context of convex programming.

The observation process is modeled as a simple linear system with additive noise, defined as:

$$\boldsymbol{f}_o(\boldsymbol{x}_k) = \boldsymbol{x}_k, \quad g_o(\boldsymbol{x}_k) = \text{blkdiag}(\sigma_r^{\text{nav}} I_3, \sigma_v^{\text{nav}} I_3), \tag{50}$$

where $\{\sigma_r^{\text{nav}}, \sigma_v^{\text{nav}}\}$ are the standard deviations of the position and velocity knowledge errors, representing OD errors. The OD windows are assumed to be available at every node, i.e., every $\sim$16.6 days (the 500-day trajectory is discretized into 31 nodes). The values of $\{\sigma_r^{\text{nav}}, \sigma_v^{\text{nav}}\}$ are assumed to be $\{\sigma_r^{\text{nav}}, \sigma_v^{\text{nav}}\} = \{200 \text{ km},\ 0.1 \text{ m/s}\}$.

Path chance constraints are imposed on the control variables, as described in Eq. (17), with the confidence level 99.9%. The state history is not constrained in the form of path constraints, but is constrained by the terminal constraints as in Eq. (18) to ensure the successful rendezvous with Mars with sufficient accuracy. $\boldsymbol{x}_f$ is defined by the ephemeris of Mars at 500 days past the departure epoch. P_f is defined as: $P_f = \text{blkdiag}(\sigma_{rf} I_3, \sigma_{vf} I_3)$, where $\{\sigma_{rf}, \sigma_{vf}\} = \{2 \times 10^3 \text{ km}, 2 \text{ m/s}\}$ are used. To avoid artificial infeasibility, the terminal constraints are relaxed and their violations are penalized via the augmented Lagrangian method.

Result Fig. 2 summarizes the result of applying our solution method to the stochastic Earth-Mars transfer problem. First, it is evident that the control profile, shown in Fig. 2(a), is largely different from Fig. 1(b). In particular, the stochastic optimal solution has smaller nominal thrust magnitude at the final approaching phase than the deterministic optimal one, implying that a margin in the nominal control profile is automatically derived by the solution method to accommodate low-thrust trajectory corrections. Conceptually, this margin is similar to a heuristic margin quantity called *forced coasting period*,[8] which is usually introduced manually at sensitive locations on low-thrust trajectories, such as before planetary rendezvous and gravity assists. The significance here is that this kind of margin quantities are discovered by the solution method with no specific inputs from mission designers, enabled by the incorporation of flight-path control planning and navigation process into the mission design framework.

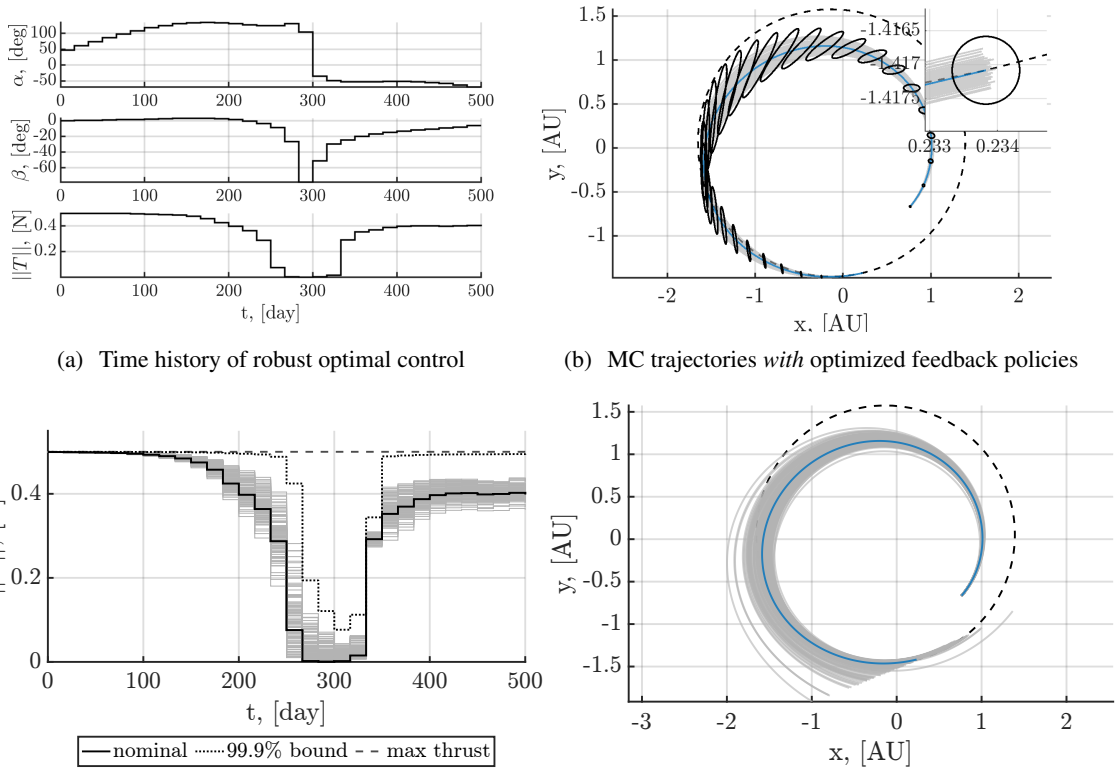

(a) Time history of robust optimal control

(b) MC trajectories *with* optimized feedback policies

(c) MC control magnitude history

(d) MC trajectories *without* trajectory corrections

Figure 2. Robust optimal Earth-Mars low-thrust transfer and Monte Carlo results

To confirm the robustness of the designed reference trajectory and associated feedback policies, nonlinear Monte Carlo (MC) simulations are performed with 100 samples, where the original nonlinear dynamics, control errors, and navigation errors are applied while the control updates are based on the linear flight-path control plan optimized by the solution method. Fig. 2(b) shows the MC result, projected on the x-y plane, where the deviation from the reference trajectory is amplified by 10 times for visualization purpose; the black ellipses overlaid represent the covariance computed inside the proposed solution method, illustrating the accuracy of UQ results performed within the optimization. The black ellipse in the zoomed view represents the covariance of the distributional constraint in Eq. (18), which confirms the successful arrival at Mars with the prescribed accuracy. Fig. 2(c) shows the history of the thrust magnitude for each of the MC sample, verifying the satisfaction of the maximum thrust constraint under the action of flight-path controls. Fig. 2(d) is included for comparison purpose, showing the result of nonlinear MC simulation *without* applying the trajectory corrections at all (again, with the amplified position deviation by a factor 10); this figure signifies the necessity of having flight-path control process.

Earth-Mars-Ceres Transfer

Transfer scenario The next transfer example is based on a recent study at JPL on the preliminary design of Earth-Mars-Ceres sample-return trajectory. In this paper, the return leg is not considered. The spacecraft is launched from Earth on 2030 Dec 18, performs a gravity assist (GA) at Mars on

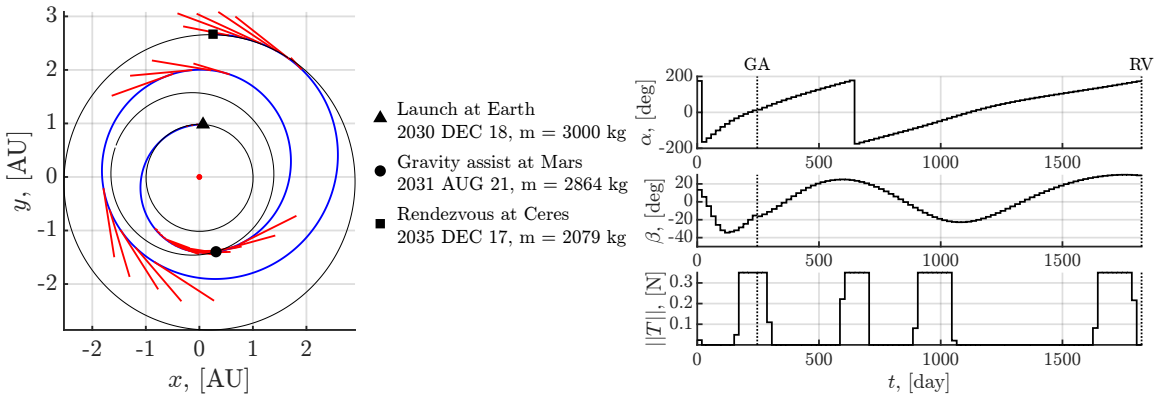

(a) Deterministic optimal trajectory

(b) Time history of deterministic optimal control

Figure 3. Deterministic optimal Earth-Mars-Ceres low-thrust transfer

2031 Aug 21, and arrives at Mars on 2035 DEC 17, with a fixed 5-year time of flight. The spacecraft specifications are assumed to be $I_{\rm sp} = 1800$ [sec], $T_{\max} = 0.35$ [N], and $m(t = 0) = 3000$ [kg]. The transfer trajectory is divided into two phases: Earth-Mars leg and Mars-Ceres leg, where the time interval between each node is set to $\sim$20 days for both legs, resulting in 14 nodes for the Earth-Mars leg and 80 nodes for the Mars-Ceres leg. Fig. 3 summarizes the deterministic optimal solution in the same manner as the Earth-Mars transfer example.

In the stochastic setting, chance constraints with 99.9% confidence level are imposed on the control magnitude and on the GA pariapsis radius, where $\mu_p = 42828\,\mathrm{km}^3/\mathrm{s}^2$, $r_{p\,\min} = 3689.5\,\mathrm{km}$ are used for Mars GA. Terminal constraints are imposed on the state statistics at the Ceres arrival, where $\{\sigma_{rf}, \sigma_{vf}\} = \{3 \times 10^3\,\mathrm{km}, 3\,\mathrm{m/s}\}$. The standard deviations of uncertain errors are assumed to be: $\{\sigma_{r0}, \sigma_{v0}\} = \{30,000\,\mathrm{km},\ 30.0\,\mathrm{m/s}\}$, $\{\sigma_r^{\rm nav}, \sigma_v^{\rm nav}\} = \{200\,\mathrm{km},\ 0.1\,\mathrm{m/s}\}$ for the first phase, $\{\sigma_r^{\rm nav}, \sigma_v^{\rm nav}\} = \{500\,\mathrm{km},\ 1\,\mathrm{m/s}\}$ for the second phase, and $\{\sigma_{\rm dire}^{\rm u}, \sigma_{\rm prop}^{\rm u}\} = \{1\,\mathrm{deg},\ 1\,\%\}$.

Result Fig. 4(a) shows the control history of the designed transfer. Like the Earth-Mars transfer example, the control profile in Fig. 4(a) is largely different from Fig. 3(b). In this transfer example, we can see that the nominal thrust level is reduced not only at the final approaching phase but also around the GA, which is also a sensitive location on the transfer trajectory. The thrust profile around the middle of the transfer indicates a less sharp behavior, for which a clear explanation has not been found yet. Finding a clear explanation of this behavior is a focus of the continued work.

Nonlinear MC simulations are performed for this transfer scenario as well. Figs. 4(b) to 4(d) show the MC result in the same manner as for the Earth-Mars transfer. Again, in Figs. 4(c) and 4(d), the deviation from the reference trajectory is amplified by 10 times for visualization purpose. Fig. 4(c) clearly demonstrates that all the MC samples are successfully controlled and arrive at Ceres with the prescribed accuracy. Figs. 4(e) and 4(f) show the distributions of the periapsis radius at the Mars GA, *with* and *without* flight path control, where $r_{p\,\min}(= 3689.5\,\mathrm{km})$ is displayed as a dashed vertical line. This clearly demonstrates the successful satisfaction of the periapsis radius constraint under uncertainty by the designed trajectory with the flight path control. On the other hand, MC simulation results without flight-path control obviously violate the terminal constraint (Fig. 4(d)) and the minimum periapsis constraint (Fig. 4(f)).

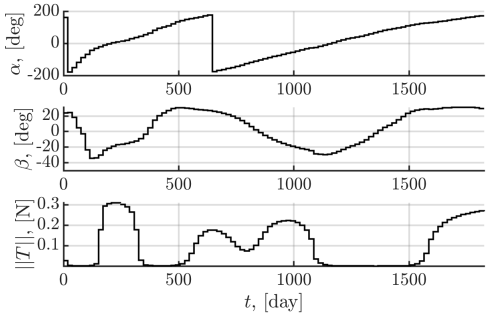

(a) Time history of robust optimal control

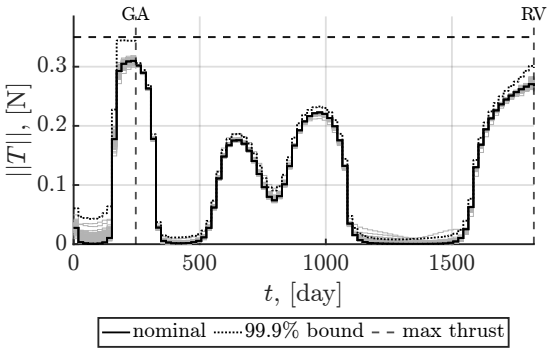

(b) MC control magnitude history

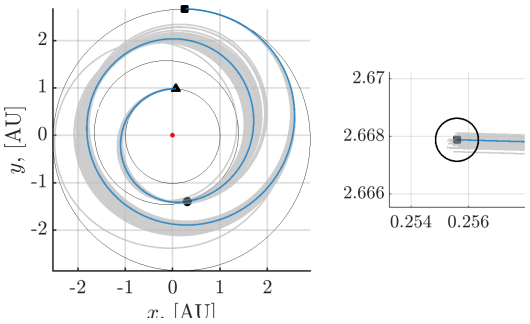

(c) MC trajectories *with* optimized feedback policies

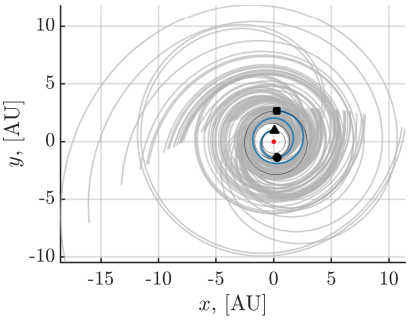

(d) MC trajectories *without* trajectory corrections

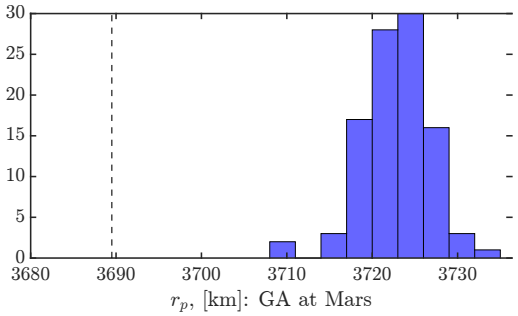

(e) GA periapris radius *with* flight path control

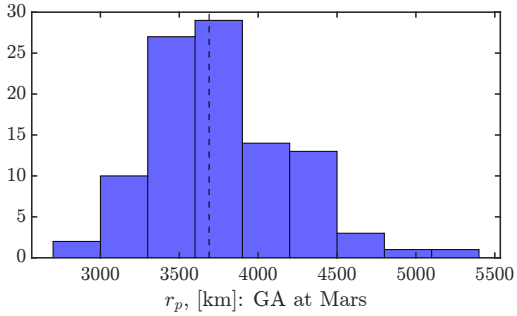

(f) GA periapris radius *without* flight path control

Figure 4. Robust optimal Earth-Mars-Ceres low-thrust transfer and Monte Carlo results

CONCLUSIONS

In this study, a mission design framework termed *Stochastic Sequential Convex Programming* is developed for robust low-thrust trajectory design under uncertainty. The developed framework combines stochastic optimal control, sequential convex programming, and the augmented Lagrangian method to incorporate the stochastic effects of orbit determination (OD) and control execution errors into the mission design process. As a result, the framework enables mission designers to concurrently design a reference trajectory and flight-path control plan such that ensure the satisfaction of mission constraints (e.g., planetary rendezvous with certain accuracy, no collision with a planet during a flyby, etc) under uncertainties due to OD errors, execution errors, and unmodeled disturbances. The proposed framework is applied to two interplanetary transfer scenarios, including

Earth-Mars transfer and Earth-Mars-Ceres transfer with an intermediate gravity assist at Mars. Nonlinear Monte Carlo simulations demonstrate the robustness of the designed reference trajectory and flight-path control under the original, nonlinear stochastic dynamics and uncertain errors. Continued development of the framework for further enhancement in terms of the efficiency and scalability is an important aspect of the ongoing work to contribute to the mission design of greater complexity.

ACKNOWLEDGMENTS

The work described in this paper was carried out in part at the Jet Propulsion Laboratory, California Institute of Technology, under a contract with National Aeronautics and Space Administration.

APPENDIX A: PROOFS

Proof of Lemma 1: Filtered state statistics equations

Proof. From Eqs. (21) and (24), the time evolution of the filtered state mean is given by:

$$\bar{\boldsymbol{x}}_{k+1} = A_k \bar{\boldsymbol{x}}_k + B_k \bar{\boldsymbol{u}}_k + \boldsymbol{h}_k,$$

which is the first equation of Eq. (26). Likewise, the covariance is calculated as:

$$\hat{P}_{k+1} = \mathbb{E}\left[(\hat{\boldsymbol{x}}_{k+1} - \bar{\boldsymbol{x}}_{k+1})(\hat{\boldsymbol{x}}_{k+1} - \bar{\boldsymbol{x}}_{k+1})^\top\right] = (A_k + B_k K_k) P_k (A_k + B_k K_k)^\top + L_{k+1} \hat{P}_{\tilde{y}_k^-} L_{k+1}^\top$$

Since $S_k S_k^\top = P_{u_k} = \mathrm{Cov}\left[\boldsymbol{u}_k\right] = \mathbb{E}\left[K_k(\hat{\boldsymbol{x}}_k - \bar{\boldsymbol{x}}_k)(\hat{\boldsymbol{x}}_k - \bar{\boldsymbol{x}}_k)^\top K_k^\top\right]$ (recall Eq. (21)), we have $S_k = K_k \hat{P}_k^{1/2} = K_k X_k$. Therefore, the covariance equation is equivalently rewritten as:

$$X_{k+1} X_{k+1}^\top = (A_k X_k + B_k S_k)(A_k X_k + B_k S_k)^\top + L_{k+1} \hat{P}_{\tilde{y}_k^-} L_{k+1}^\top,$$

which is implied by the second equation of Eq. (26). □

Proof of Lemma 2: Three-dimensional control magnitude chance constraint

Proof. Since $\boldsymbol{u} \sim \mathcal{N}(\bar{\boldsymbol{u}}, P_u)$, $\boldsymbol{u}$ can be written as $\boldsymbol{u} = \bar{\boldsymbol{u}} + P_u^{1/2}\boldsymbol{v}$, where $\boldsymbol{v} \sim \mathcal{N}(0, I_{n_u})$. Applying the triangle inequality yields $\|\boldsymbol{u}\|_2 \le \|\bar{\boldsymbol{u}}\|_2 + \|P_u^{1/2}\boldsymbol{v}\|_2 \le \|\bar{\boldsymbol{u}}\|_2 + \|P_u^{1/2}\|_2 \|\boldsymbol{v}\|_2$, which implies

$$\mathbb{P}\left[\|\boldsymbol{u}\|_2 \le u_{\max}\right] \ge \mathbb{P}\left[\|\bar{\boldsymbol{u}}\|_2 + \|P_u^{1/2}\|_2 \|\boldsymbol{v}\|_2 \le u_{\max}\right] = \mathbb{P}\left[\|\boldsymbol{v}\|_2 \le (u_{\max} - \|\bar{\boldsymbol{u}}\|_2)/\|P_u^{1/2}\|_2\right].$$

Here, since $\boldsymbol{v} \sim \mathcal{N}(0, I_{n_u})$, $\|\boldsymbol{v}\|_2^2$ is subject to $\chi^2(n_u)$ (i.e., chi-squared distribution with n_u degrees of freedom), and hence, for a deterministic quantity $v_{\max} \ge 0$, we have

$$\begin{aligned}\mathbb{P}\left[\|\boldsymbol{v}\|_2 \le v_{\max}\right] = \mathbb{P}\left[\|\boldsymbol{v}\|_2^2 \le v_{\max}^2\right] \ge 1-\varepsilon \;&\Leftrightarrow\; Q_{X\sim\chi^2(n_u)}(1-\varepsilon) \le v_{\max}^2 \\ &\Leftrightarrow\; \sqrt{Q_{X\sim\chi^2(n_u)}(1-\varepsilon)} \le v_{\max}\end{aligned}$$

where $Q_{X\sim\chi^2(n_u)}(\cdot)$ is the quantile function of a $\chi^2(n_u)$-random variable. Therefore,

$$\begin{aligned}\mathbb{P}\left[\|\boldsymbol{u}\|_2 \le u_{\max}\right] \ge 1-\varepsilon \;&\Leftarrow\; \mathbb{P}\left[\|\boldsymbol{v}\|_2 \le (u_{\max} - \|\bar{\boldsymbol{u}}\|_2)/\|P_u^{1/2}\|_2\right] \ge 1-\varepsilon \\ &\Leftrightarrow\; \sqrt{Q_{X\sim\chi^2(n_u)}(1-\varepsilon)} \le \frac{u_{\max} - \|\bar{\boldsymbol{u}}\|_2}{\|P_u^{1/2}\|_2},\end{aligned}$$

which, noting the identity $\|P_u^{1/2}\|_2 = \sqrt{\lambda_{\max}(P_u)}$, is equivalent to Eq. (33). □

Proof of Lemma 3: Mass variable quantile function

Proof. Using Eqs. (15) and (37), $Q_{z_k}(1-\varepsilon_u/2)$ is calculated as:

$$\begin{aligned} Q_{z_k}\left(1-\frac{\varepsilon_u}{2}\right) &= \min\left\{ z \mid \mathbb{P}\left[z_0 - \sum_{i=0}^{k-1} b_i \|\boldsymbol{u}_i\|_2 \le z \right] \ge 1-\frac{\varepsilon_u}{2} \right\} \\ &= \min\left\{ z_0 - \Delta z \mid \mathbb{P}\left[\Delta z \le \sum_{i=0}^{k-1} b_i \|\boldsymbol{u}_i\|_2 \right] \ge 1-\frac{\varepsilon_u}{2} \right\} \\ &= \min\left\{ z_0 - \sum_{i=0}^{k-1} \Delta z_i \mid \mathbb{P}\left[\bigwedge_{i=0}^{k-1} (\Delta z_i \le b_i \|\boldsymbol{u}_i\|_2) \right] \ge 1-\frac{\varepsilon_u}{2} \right\}, \end{aligned}$$

where $\Delta z = \sum_{i=0}^{k-1} \Delta z_i = z_0 - z$ and $\Delta z_i \ge 0$. It follows that by applying the Boole's inequality,[21]

$$\begin{aligned} Q_{z_k}\left(1-\frac{\varepsilon_u}{2}\right) &\le \min\left\{ z_0 - \sum_{i=0}^{k-1} \Delta z_i \mid \bigwedge_{i=0}^{k-1} \left(\mathbb{P}\left[\Delta z_i \le b_i \|\boldsymbol{u}_i\|_2 \right] \ge 1-\frac{\varepsilon_u}{2k} \right) \right\} \\ &= z_0 - \sum_{i=0}^{k-1} \max\left\{ \Delta z_i \mid \bigwedge_{i=0}^{k-1} \left(\mathbb{P}\left[\Delta z_i \le b_i \|\boldsymbol{u}_i\|_2 \right] \ge 1-\frac{\varepsilon_u}{2k} \right) \right\}, \end{aligned} \tag{51}$$

where the risk $\varepsilon_u/2$ is equally allocated for each of $i = 0, 1, ..., k-1$ (uneven risk allocation is also possible). Here, noting $\boldsymbol{u}_i = \bar{\boldsymbol{u}}_i + P_{u_i}^{1/2}\boldsymbol{v}$, where $\boldsymbol{v} \sim \mathcal{N}(0, I_{n_u})$, $\|\boldsymbol{u}_i\|_2$ can be evaluated from below by using the (reverse) triangle inequality as:

$$\|\boldsymbol{u}\|_2 \ge \left| \|\bar{\boldsymbol{u}}\|_2 - \|P_{u_i}^{1/2}\boldsymbol{v}\|_2 \right| \ge \max\{0, \|\bar{\boldsymbol{u}}\|_2 - \|P_{u_i}^{1/2}\boldsymbol{v}\|_2\} \ge \max\{0, \|\bar{\boldsymbol{u}}\|_2 - \|P_{u_i}^{1/2}\|_2 \|\boldsymbol{v}\|_2\}$$

Using this, the chance constraint in the last line of Eq. (51) can be evaluated as:

$$\begin{aligned} \mathbb{P}\left[\Delta z_i \le b_i \|\boldsymbol{u}_i\|_2 \right] &\ge \mathbb{P}\left[\Delta z_i \le b_i \max\{0, \|\bar{\boldsymbol{u}}\|_2 - \|P_{u_i}^{1/2}\|_2 \|\boldsymbol{v}\|_2\} \right] \ge 1-\frac{\varepsilon_u}{2k} \\ &\Leftarrow \Delta z_i \le b_i \max\left\{ 0, \|\bar{\boldsymbol{u}}\|_2 - n_\sigma\left(\frac{\varepsilon_u}{2k}, n_u\right) \|P_{u_i}^{1/2}\|_2 \right\} \end{aligned} \tag{52}$$

where $n_\sigma(\cdot,\cdot)$ is as defined in Eq. (32). Therefore, combining Eqs. (51) and (52), we have

$$\begin{aligned} Q_{z_k}\left(1-\frac{\varepsilon_u}{2}\right) &\le z_0 - \sum_{i=0}^{k-1} \max\left\{ \Delta z_i \mid \bigwedge_{i=0}^{k-1} \left(\Delta z_i \le b_i \max\left\{ 0, \|\bar{\boldsymbol{u}}\|_2 - n_\sigma\left(\frac{\varepsilon_u}{2k}, n_u\right) \|P_{u_i}^{1/2}\|_2 \right\} \right) \right\} \\ &= z_0 - \sum_{i=0}^{k-1} b_i \max\left\{ 0, \|\bar{\boldsymbol{u}}\|_2 - n_\sigma\left(\frac{\varepsilon_u}{2k}, n_u\right) \|P_{u_i}^{1/2}\|_2 \right\}, \end{aligned}$$

completing the proof (note the identity $\|P_u^{1/2}\|_2 = \sqrt{\lambda_{\max}(P_u)}$). □

REFERENCES

[1] D. F. Lawden, "General Theory of Optimal Rocket Trajectories," *Optimal trajectories for space navigation*, ch. 3, London: Butterworths, dec 1963.

[2] R. P. Russell, "Primer Vector Theory Applied to Global Low-Thrust Trade Studies," *Journal of Guidance, Control, and Dynamics*, Vol. 30, mar 2007, pp. 460–472, 10.2514/1.22984.

[3] S. B. GERSHWIN and D. H. JACOBSON, "A discrete-time differential dynamic programming algorithm with application to optimal orbit transfer," *AIAA Journal*, Vol. 8, sep 1970, pp. 1616–1626, 10.2514/3.5955.

[4] G. Lantoine and R. P. Russell, "A Hybrid Differential Dynamic Programming Algorithm for Constrained Optimal Control Problems. Part 1: Theory," *Journal of Optimization Theory and Applications*, Vol. 154, aug 2012, pp. 382–417, 10.1007/s10957-012-0039-0.

[5] J. T. Betts, "3. Optimal Control Preliminaries," *Practical Methods for Optimal Control and Estimation Using Nonlinear Programming*, ch. 3, pp. 91–121, Society for Industrial and Applied Mathematics, jan 2010, 10.1137/1.9780898718577.ch3.

[6] C. Hargraves and S. Paris, "Direct Trajectory Optimization Using Nonlinear Programming and Collocation," *Journal of Guidance, Control, and Dynamics*, Vol. 10, jul 1987, pp. 338–342, 10.2514/3.20223.

[7] D. Oh, D. Landau, T. Randolph, P. Timmerman, J. Chase, J. Sims, and T. Kowalkowski, "Analysis of System Margins on Deep Space Missions Using Solar Electric Propulsion," *44th AIAA/ASME/SAE/ASEE Joint Propulsion Conference and Exhibit*, No. July, Reston, Virigina, American Institute of Aeronautics and Astronautics, jul 2008, pp. 1–30, 10.2514/6.2008-5286.

[8] M. D. Rayman, T. C. Fraschetti, C. A. Raymond, and C. T. Russell, "Coupling of system resource margins through the use of electric propulsion: Implications in preparing for the Dawn mission to Ceres and Vesta," *Acta Astronautica*, Vol. 60, No. 10-11, 2007, pp. 930–938, 10.1016/j.actaastro.2006.11.012.

[9] N. Ozaki, S. Campagnola, and R. Funase, "Tube Stochastic Optimal Control for Nonlinear Constrained Trajectory Optimization Problems," *Journal of Guidance, Control, and Dynamics*, Vol. 43, apr 2020, pp. 645–655, 10.2514/1.G004363.

[10] C. Greco, M. Di Carlo, M. Vasile, and R. Epenoy, "Direct multiple shooting transcription with polynomial algebra for optimal control problems under uncertainty," *Acta Astronautica*, Vol. 170, may 2020, pp. 224–234, 10.1016/j.actaastro.2019.12.010.

[11] J. Ridderhof, J. Pilipovsky, and P. Tsiotras, "Chance-constrained Covariance Control for Low-Thrust Minimum-Fuel Trajectory Optimization," *AAS/AIAA Astrodynamics Specialist Conference*, South Lake Tahoe, CA (Virtual), AAS, aug 2020.

[12] K. Oguri and J. W. McMahon, "Stochastic Primer Vector for Robust Low-Thrust Trajectory Design Under Uncertainty," *Journal of Guidance, Control, and Dynamics*, Vol. 45, jan 2022, pp. 84–102, 10.2514/1.G005970.

[13] K. Oguri, G. Lantoine, and T. H. Sweetser, "Robust Solar Sail Trajectory Design under Uncertainty with Application to NEA Scout Mission," *AIAA SCITECH Forum*, Reston, Virginia, American Institute of Aeronautics and Astronautics, jan 2022, pp. 1–20, 10.2514/6.2022-1627.

[14] B. Benedikter, A. Zavoli, Z. Wang, S. Pizzurro, and E. Cavallini, "Covariance Control for Stochastic Low-Thrust Trajectory Optimization," *AIAA SCITECH 2022 Forum*, Reston, Virginia, American Institute of Aeronautics and Astronautics, jan 2022, pp. 1–19, 10.2514/6.2022-2474.

[15] B. Acikmese and S. R. Ploen, "Convex Programming Approach to Powered Descent Guidance for Mars Landing," *Journal of Guidance Control and Dynamics*, Vol. 30, No. 5, 2007, p. 1353, 10.2514/1.27553.

[16] C. R. Gates, "A simplified model of midcourse maneuver execution errors," tech. rep., Jet Propulsion Laboratory, California Institute of Technology (Report No. 32-504), Pasadena, CA, oct 1963.

[17] J. Ridderhof, K. Okamoto, and P. Tsiotras, "Chance Constrained Covariance Control for Linear Stochastic Systems With Output Feedback," *2020 59th IEEE Conference on Decision and Control (CDC)*, Vol. 2020-Decem, IEEE, dec 2020, pp. 1758–1763, 10.1109/CDC42340.2020.9303731.

[18] Y. Mao, M. Szmuk, X. Xu, and B. Acikmese, "Successive Convexification: A Superlinearly Convergent Algorithm for Non-convex Optimal Control Problems," *arXiv preprint*, apr 2018, pp. 1–35.

[19] M. Szmuk, T. P. Reynolds, and B. Açıkmeşe, "Successive Convexification for Real-Time Six-Degree-of-Freedom Powered Descent Guidance with State-Triggered Constraints," *Journal of Guidance, Control, and Dynamics*, Vol. 43, aug 2020, pp. 1399–1413, 10.2514/1.G004549.

[20] K. Oguri and J. W. McMahon, "Stochastic Primer Vector for Robust Impulsive Trajectory Design Under Uncertainty," *AAS/AIAA Astrodynamics Specialist Conference*, South Lake Tahoe, CA (Virtual), aug 2020.

[21] A. Prekopa, "Boole-Bonferroni Inequalities and Linear Programming," *Operations Research*, Vol. 36, No. 1, 1988, pp. 145–162.

[22] D. P. Bertsekas, *Constrained Optimization and Lagrange Multiplier Methods*. Elsevier, 1982, 10.1016/C2013-0-10366-2.

[23] J. A. Sims, *Delta-V Gravity-Assist Trajectory Design: Theory and Practice*. PhD thesis, 1996.

[24] D. H. Ellison and J. A. Englander, "High-Fidelity Multiple-Flyby Trajectory Optimization Using Multiple Shooting," *2AAS/AIAA Astrodynamics Specialist Conference*, Portland, ME, aug 2019.